Optimization of Structures in Composite Reinforced by Fiber and Bidimensional Additive Processes

Pedro Miguel Alves da Costa
pedro.a.costa@tecnico.ulisboa.pt

Instituto Superior Técnico, Universidade de Lisboa, Portugal

December 2019

Abstract

The development of continuous fiber filament technology in the FFF process enabled the production of lighter, stronger structural parts. In order to develop optimal structures using this technology, this work aims to optimize the material distribution and orientation of bidimensional structures produced by fused filament fabrication using continuous fiber. The design optimization is performed using the DMO method with the optimized structures being printed using the Markforged Mark Two 3D printer. Computed and experimental results show the effect of using different optimization and printing parameters.

Keywords: Discrete Material Optimization (DMO), Markforged Mark Two, Fiber orientation optimization, Additive Manufacturing, Fiber Reinforced Composite structures

1. Introduction

Additive manufacturing (AM) technologies have found potential applications in various industries such as the aerospace and automotive industries by allowing the creation of complex lightweight structures. These technologies allow the fabrication of prototypes or functional components with complex structures such as those obtained by topology optimization, which could be too expensive to manufacture by conventional methods, and also difficult, if not impossible [3].

One of these technologies is the Fused Filament Fabrication (FFF) method which consists in reproducing a three-dimensional geometry through the deposition of successive layers of extruded thermoplastic filament. This technology has become widely adopted due to its low cost, low material wastage and ease of use. The most common materials used by this process include Polycarbonate (PC), Polylactic acid (PLA), Acrylonitrile butadiene styrene (ABS) and Polyamide (PA or Nylon), due to their low cost and low melting temperature [5]. However, the poor mechanical properties of parts printed using these materials results in the FFF process being primarily used to develop prototypes [4]. In order to improve the mechanical properties of 3D printed parts, the combination of a polymeric matrix with reinforcements such as particles, fibers and nano-materials allows the manufacture of structural parts, characterized by their high-performance and functionality [3]. These advantages lead to the recent development of 3D printing technology of Fiber Reinforced Thermoplastic Composite (FRTPC) structures using short and continuous fibers. An example of the materials used are carbon fiber, fiberglass and Kevlar.

Although the use of fibers tends to improve the overall strength and stiffness of parts produced by Fused Filament Fabrication, this improvement is only relevant when the fibers are oriented towards the stresses that the part is set upon. Also, the use of these materials greatly increases the cost of production, resulting in the need for them to be used efficiently.

For these reasons, this work aims to optimize in terms of stiffness both the topology and material orientation of parts produced by FFF technology using continuous fiber as reinforcement.

Studies about structural optimization using continuous fiber can be seen in references [8], [10] and [11], with the FFF process being also considered in references [7] and [9].

2. Optimization

Assuming that all materials have a linear elastic behavior, the structural optimization problem of maximizing the stiffness of a structure can be reformulated as minimizing the displacements caused by applied loads on the structure, in what is known as minimizing the structural compliance $\mathcal{C}$. By using the finite element method to analyze the loaded structure, the optimization problem can be stated

as

$$\begin{aligned} \text{Minimize} \quad & \mathcal{C}(x) = \mathbf{p}^T \mathbf{u} \\ \text{subject to} \quad & \mathbf{K}\,\mathbf{u} = \mathbf{p} \\ & m \leq m_c \\ & 0 \leq x_{min} \leq x \leq 1 \end{aligned} \tag{1}$$

where $\mathbf{p}$ is the applied forces vector, $\mathbf{u}$ is the displacement vector, $\mathbf{K}$ is the stiffness matrix, m is the mass of the structure, m_c is the allowed total mass and x are the design variables of the optimization problem.

The optimization method applied in this work is known as Discrete Material Optimization (DMO) method, developed by Stegmann[15] in order to avoid local minima solutions encountered by other material orientation optimization methods, such as the Continuous Fiber Angle Optimization (CFAO) method. This parametrization method computes the element constitutive matrix $\mathbf{C^e}$ as a sum of constitutive matrix $\mathbf{C}_i$ over the number of candidate materials, n^e:

$$\mathbf{C}^e = \sum_{i=1}^{n^e} w_i \mathbf{C}_i = w_1 \mathbf{C}_1 + \ldots + w_{n^e} \mathbf{C}_{n^e} \tag{2}$$
$$0 \leq w_i \leq 1$$

with each matrix $\mathbf{C}_i$ corresponding to a discrete candidate material and being affected by a weight function w_i. By using continuous weight functions, gradient based optimizers can be applied in the optimization despite the use of discrete candidate materials. In order for the design to be physically possible, the weight functions must have values between 0 and 1. Several parametrizations have been developed for the DMO method based on these conditions [15]. One of the most efficient can be formulated as:

$$\mathbf{C^e} = \sum_{i=1}^{n^e} \underbrace{\left[(x_i^e)^p \prod_{j=1; j\neq i}^{n^e} \left[1 - (x_j^e)^p\right]\right]}_{w_i} \mathbf{C}_i \tag{3}$$

with the design variables x_i, $i = 1, \ldots, n^e$ being pushed to the values of 0 and 1 by adopting the penalization factor p from the SIMP method, which penalizes intermediate values of x_i. Despite the efficiency of this parametrization, during the optimization the sum of the weight functions can be different than one, i.e. $\sum w_i \neq 1$, which raises issues when computing the mass of the structure:

$$m = \sum_{e=1}^{N^e} \sum_{i=1}^{n^e} (w_i \rho_i V)^e \tag{4}$$

where N^e is the total number of finite elements, ρ_i is the density of the candidate material and V is the finite element's volume. This can be resolved by normalizing the weight functions, resulting in the parametrization:

$$w_i = \frac{w_k}{\sum_{k=1}^{n^e} w_k} \tag{5}$$

in which the weight functions w_k are computed using the parametrization in (3). This normalization reduces the effectiveness of the penalization in penalizing intermediate values of x_i. As such, the parametrization presented in (3) is used for the element constitutive matrix $\mathbf{C^e}$, while (5) is used for the computation of the mass of the structure.

In order to update the design variables, the gradients of the objective and constraints need to be computed. By rewriting the compliance $\mathcal{C}$ as:

$$\mathcal{C}(x) = \mathbf{u}^T\ \mathbf{K}\ \mathbf{u} \tag{6}$$

and differentiating with respect to x_i, assuming that $\partial \mathbf{p}^T / \partial x_i = 0$, the compliance sensitivity can be written as:

$$\frac{d\mathcal{C}}{dx_i} = -\mathbf{u}^T \frac{\partial \mathbf{K}}{\partial x_i} \mathbf{u} \tag{7}$$

with the stiffness matrix $\mathbf{K}$ defined as:

$$\mathbf{K} = \sum_{e=1}^{N^e} \int_{V^e} (\mathbf{B}^e)^T\, \mathbf{C}^e\, \mathbf{B}^e\ dV \tag{8}$$

where $\mathbf{B}^e$ is the element strain-displacement matrix. The constitutive matrix $\mathbf{C}$ of each candidate material in (2) is defined as:

$$\mathbf{C} = \begin{bmatrix} \dfrac{E_1}{1-\nu_{12}\nu_{21}} & \dfrac{\nu_{12}E_2}{1-\nu_{12}\nu_{21}} & 0 \\ \dfrac{\nu_{21}E_1}{1-\nu_{12}\nu_{21}} & \dfrac{E_2}{1-\nu_{12}\nu_{21}} & 0 \\ 0 & 0 & G_{12} \end{bmatrix} \tag{9}$$

in the case of an orthotropic material using the principal material directions. In order to write the constitutive matrix in the problem's system of coordinates, the transformation of coordinates

$$\bar{\mathbf{C}} = \mathbf{T}(\theta)\, \mathbf{C}\, \mathbf{T}(\theta)^T \tag{10}$$

is performed with $\mathbf{T}(\theta)$ written as:

$$\mathbf{T}(\theta) = \begin{bmatrix} \cos^2\theta & \sin^2\theta & -2\cos\theta\sin\theta \\ \sin^2\theta & \cos^2\theta & 2\cos\theta\sin\theta \\ \cos\theta\sin\theta & -\cos\theta\sin\theta & \cos^2\theta - \sin^2\theta \end{bmatrix} \tag{11}$$

Obtaining the gradient in (7) thus only requires calculating the derivatives of the weighting functions in (3). To compute the constraint function sensitivity, the necessary derivatives relate to the weighting function in (5).

To prevent checkerboard results and avoid mesh dependency, a density filter is used [14], in which the filtered design variables are written as:

$$\tilde{x}_{ec} = \frac{\sum_{i\in\mathbb{N}_e} \mathrm{w}^e(\mathbf{x}_i) V_i x_{ic}}{\sum_{i\in\mathbb{N}_e} \mathrm{w}^e(\mathbf{x}_i) V_i}; \qquad \forall(e,c) \tag{12}$$

where $\mathbb{N}_e$ are the elements inside the filter radius, r, relative to the e'th element, V_i is the volume of the i'th element, x_{ic} is the non-filtered design variable relative to the i'th element and unique candidate material c and $\mathrm{w}^e(\mathbf{x}_i)$ is a standard linear decaying weight function defined as:

$$\mathrm{w}^e(\mathbf{x}_i) = 1 - \frac{\|\mathbf{x}_i - \mathbf{x}_e\|}{r} \tag{13}$$

in which the term $\|\mathbf{x}_i - \mathbf{x}_e\|$ is the distance between the center points of the i'th and e'th elements based on the Euclidean norm of the vectors containing the coordinates of these points.

To determine convergence of the optimization, the relative change of the design variables is calculated as

$$R = \sqrt{\frac{\sum_{i=1}^{N^e}\sum_{c=1}^{n^e}(x_{ic}^{n+1} - x_{ic}^{n})^2}{\sum_{i=1}^{N^e}\sum_{c=1}^{n^e}(\overline{x}_{ic} - \underline{x}_{ic})^2}} \tag{14}$$

where n is the number of the current iteration, $\overline{x}_{ic}$ and $\underline{x}_{ic}$ are the upper and lower bounds of the i'th element and c'th discrete material, i.e., 1 and 0, respectively. If R is below the established threshold, e.g. $R = 0.01$ if the relative change of the design variables should be below 1%, or if the value of the objective function didn't change significantly, the optimization is considered to have converged numerically. This solution could, however, still be unacceptable, or still have room for improvement.

To confirm that the optimization has achieved a satisfactory solution, i.e., a single material has been selected in all the elements, a DMO convergence measure is implemented from [15]. First, the convergence for each element is measured, by comparing the Euclidean norm of the weight factors for each weight factor, w_i:

$$w_i \geq \epsilon\sqrt{w_1^2 + w_2^2 + \cdots + w_{n^e}^2} \tag{15}$$

where ϵ is a tolerance level, with typical values ranging between 95% - 99.5%. If the inequality in (15) is satisfied, the element is flagged as converged. After analyzing the convergence of all elements, the DMO convergence (also known as the solution discreteness), h_ϵ, can be calculated by dividing the number of converged elements, N_c^e, by the number of total elements, N^e,

$$h_\epsilon = \frac{N_c^e}{N^e} \tag{16}$$

with full convergence considered to have been achieved when $h_\epsilon = 1$.

If the DMO convergence is above an imposed minimum, the solution is considered satisfactory. However, if the non-discreteness of the solution is deemed unacceptable and the penalization power p is below p_{max}, the optimization is reinitialized with an increased penalization.

3. Implementation

In order to implement the DMO method into a finite element program, a custom MATLAB program was developed capable of dealing with generic bidimensional finite meshes composed of linear triangular and quadrilateral elements. The finite element data is provided in a .dat file generated in the commercial finite element software Siemens NX. This file contains the pre-processed design information such as nodes, elements, elemental connectivity matrix and boundary conditions of the design problem. The program reads this data and then proceeds to initiate the optimization routine by computing the finite element analysis and sensitivity analysis whose results are used to calculate the compliance and design gradients. The optimization problem is then solved using the MMA optimization algorithm developed and provided by Svanberg[16].

3.1. Computational Results

To test the applicability of the DMO method for material distribution and fiber angle optimizations, a series of optimizations focused on the so-called Messerschimitt-Bölkow-Blohm (MBB) beam [12] and on a three-point tensile (3PT) example (see Fig. 1) are presented. The goal of these optimizations serves to understand the influence of certain parameters in the final optimal structure. In the former example, the change in material properties are studied and in the latter, the study is focused on the change in the mass constraint and its effects in the final compliance. In the optimization results, the presence of fiber material is represented by a darker element with a dash symbolizing the material orientation, while the solid, lighter elements represent void material. Black and white elements represent converged elements, while an intermediate, gray color represents unconverged elements.

3.1.1. MBB beam optimization

In the following optimizations, the mass constraint is set at 50% of the maximum mass and a filter radius of $r = 1.4$ mm is used. The starting penalization is set as $p = 3$, increasing by 4 up to a maximum of $p = 23$, if the convergence requirements of a minimum of 95% converged elements aren't met. These requirements are tested when the relative change of the design values is below $R = 0.005 = 0.5\%$ or the change in com-

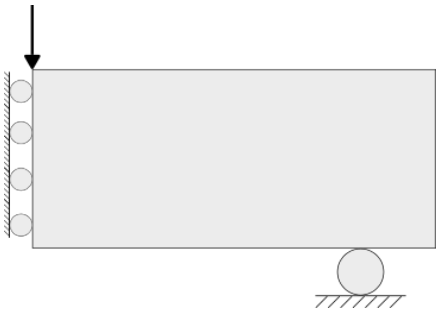

(a) MBB half-beam design space and loading conditions

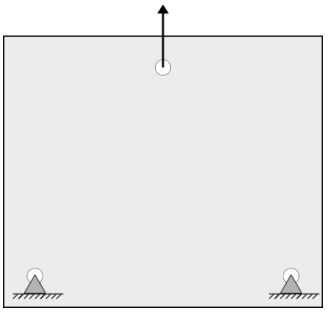

(b) 3PT design space and loading conditions

Figure 1: Design space and loading conditions for the MBB beam and 3PT optimizations

pliance is below 0.001%. The dimensions of the full beam are 180 × 40 [mm] with a total thickness of 1 mm. The beam is supported on the bottom edge at two symmetrically placed points, 10 mm inwards from the lateral edges, fixing the vertical displacement at those points. A single 1 Newton downward load is applied at the top center of the structure. The MBB half-beam is modeled using 90 by 40 elements and there are 8 possible orientations $[90°, \pm 67.5°, \pm 45°, \pm 22.5°, 0°]$ for the orthotropic material. The first set of optimizations focused on changing the Young's modulus ratio by decreasing E_2 while maintaining the value of E_1. The optimization results can be observed in Fig. 2 for $E_1/E_2 = 1$, 2 and 10.

With exception of using $E_1/E_2 = 1$, which corresponds to an isotropic material, changing the Young's modulus ratio has no significant influence in the material distribution.

The next set of optimizations focused on understanding the influence of changing the shear modulus of the orthotropic material. The shear stiffness is measured by the β parameter [13, 2], which can be stated as:

$$\beta = \frac{E_1}{1 - \nu_{12}\nu_{21}} + \frac{E_2}{1 - \nu_{12}\nu_{21}} - 2\frac{\nu_{12}E_2}{1 - \nu_{12}\nu_{21}} - 4G_{12} \tag{17}$$

with most materials being characterized as weak in shear, $\beta \geq 0$, with isotropic materials having $\beta = 0$. Materials with $\beta < 0$ are considered strong in shear. The optimization results for optimizations with different values of β can be observed in Fig. 3.

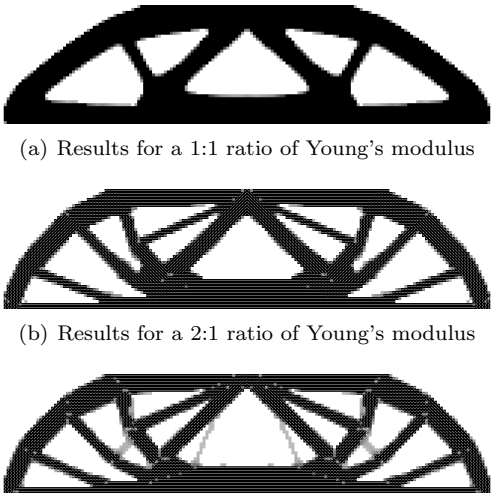

(a) Results for a 1:1 ratio of Young's modulus

(b) Results for a 2:1 ratio of Young's modulus

(c) Results for a 10:1 ratio of Young's modulus

Figure 2: Results for the full MBB beam optimization problem using the DMO method for different ratios of Young's modulus

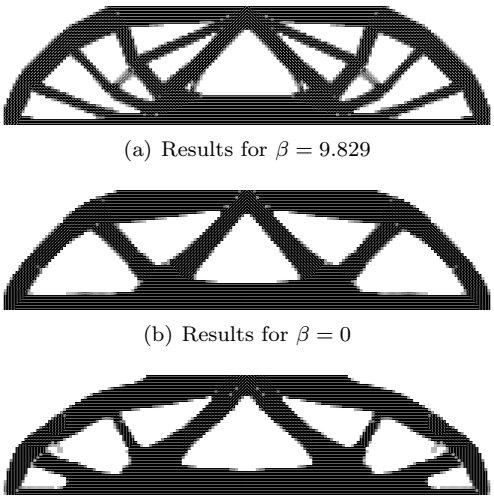

(a) Results for $\beta = 9.829$

(b) Results for $\beta = 0$

(c) Results for $\beta = -4.571$

Figure 3: Results for the full MBB beam optimization problem using the DMO method for different β values

In this case, changing the shear modulus has severe influence in the material distribution and orientation, with the material distribution for $\beta = 0$ being similar to the isotropic material distribution in Fig. 2(a) and for $\beta < 0$, the material orientation does not correspond with the principal stress directions in the structure's members.

3.1.2. 3PT optimization

In this optimization problem, the material distribution and orientation as well as structural stiffness for different mass constraints are evaluated. The design domain represented in Fig. 1(b) consists of a rectangle with dimensions 100 × 85 [mm] with a thickness of 1 mm. It has three centered Ø5 mm holes, two aligned at the bottom situated 80 mm apart and one at the top, 65 mm vertically from the others. A 1 Newton bearing force is applied upwards in the top hole while the remaining holes remain fixed in the horizontal and vertical directions. Using the same optimization parameters as implemented in section 3.1.1 and an orthotropic material with $E_1 = 10$ MPa, $E_2 = 2.5$ MPa, $G_{12} = 0.4$ MPa and $\nu_{12} = 0.25$ oriented at $[90°, \pm 67.5°, \pm 45°, \pm 22.5°, 0°]$, the optimization results for different mass constraints can be observed in Fig. 4 and Table 1. The results indicate that as

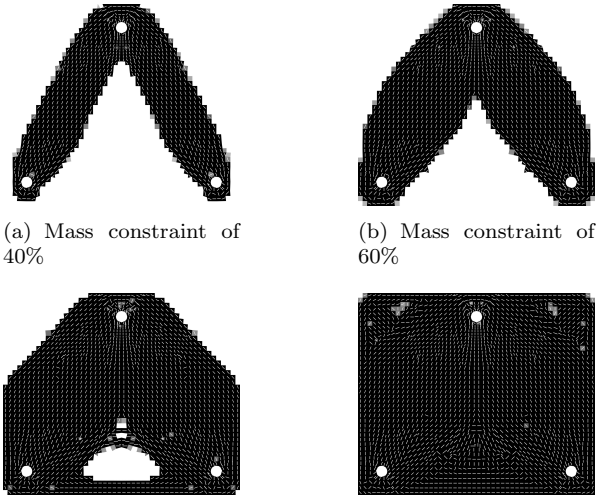

(a) Mass constraint of 40%

(b) Mass constraint of 60%

(c) Mass constraint of 80%

(d) Mass constraint of 100%

Figure 4: Results for the three-point tensile optimization using different mass constraints

Table 1: Three-point tensile optimization results for different mass constraints

Mass %	Final Compliance [N.m] $\times 10^{-3}$	Normalized Compliance [N.m] $\times 10^{-3}$
40	2.368	0.936
60	2.009	1.191
80	1.946	1.547
100	1.957	1.957

the mass constraint increases, the compliance of the structure decreases. Although heavier structures should be stiffer, differences in material orientation also have an effect in the compliance value as can be observed in the 80% structure which presents the lowest compliance value. By multiplying the compliance with the mass constraint of the structure and dividing by the weightiest structure's mass constraint, the normalized compliance can be determined. The results in this case indicate that by decreasing the mass constraint, decreasing the allowed mass, the normalized compliance decreases as well, resulting in a better stiffness/weight ratio.

4. Experimental Setup

In order to validate the computational results for optimal material distribution and orientation using the DMO method, experimental tests in structures printed using continuous fiber fabrication technology are performed. The structures are printed with a Markforged Mark Two 3D printer using a sandwich panel design with the outer layers reinforced with fiberglass and a triangular nylon core. The material properties of the sandwich panel are obtained by the testing of tensile specimens. The goal of the MBB beam experimental testing is to compare the stiffness of similarly weighted topology optimized structures with topology and material orientation optimized structures. In the 3-point tensile experimental testing, the goal is to compare quasi-isotropic structures against structures with optimized material orientation for different volume fractions. These tests serve to understand the advantages and disadvantages of topology optimization vs topology and material orientation optimization using CFF and also advantages and disadvantages of printed laminated, quasi-isotropic structures vs printed structures with optimized material orientation in the context of CFF.

In order to be able to establish a comparison between the computational and experimental results, the mechanical properties of the sandwich panels are obtained using a unidirectional layered sandwich panel [6] following the ASTM D3039 standard [1].

These properties are obtained for an orthotropic laminate and a quasi-isotropic laminate, to use in material distribution with orientation optimization and in topology optimization, respectively. Each laminate has a thickness of 5mm and 8 fiber layers. The obtained properties can be seen in Tables 2 and 3.

Using the obtained mechanical properties, the final optimal designs for the test studies can be seen in Figs. 5 and 6 which are then printed and tested.

4.1. MBB beam experimental setup and results

Both MBB structures are printed using *Concentric* fiber fill, to compare the stiffness of the structures obtained through the optimizations with the fiber oriented according to the principal stress directions.

Table 2: In-plane tensile properties for the unidirectional composite sandwich panel

Property	Value
E_1 (GPa)	3.869
E_2 (GPa)	0.356
G_{12} (GPa)	0.742
ν_{12}	0.426
ν_{21}	0.022

Table 3: In-plane tensile properties for the *Isotropic* composite sandwich panel

Property	Value
E (GPa)	1.513
ν	0.394

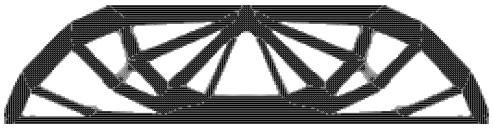

(a) Final optimal material and fiber angle distribution for the *MBB_ORTHO* optimization

(b) Final optimal material distribution for the *MBB_ISO* optimization

Figure 5: Final optimal material distribution and orientation results for the *MBB_ORTHO* and *MBB_ISO* optimizations

In order to improve the stability of the structure during the tests, the structures are printed with a thickness of 10mm and 16 fiber layers, to maintain the fiber/nylon ratio used in the tensile specimens. The experimental setup can be seen in Fig. 7.

The results of the experiment can be seen in Fig. 8 and Table 4.

From the analysis of the experimental stiffness results, the structures seem to have similar stiffness, with the *MBB_ISO* having a greater variation in results and an overall better performance. These experimental results contradict the theoretical results obtained through the optimizations. These differences can be related to the printing patterns, which cannot be replicated through the optimization program.

4.2. 3PT experimental setup and results

For this experiment, the 3PT structures are printed using Markforged's *Concentric* and *Isotropic* fiber fill, to compare the stiffness of structures printed with the fibers aligned with the principal stress directions and structures printed with a quasi-isotropic laminate, optimized for different mass constraints.

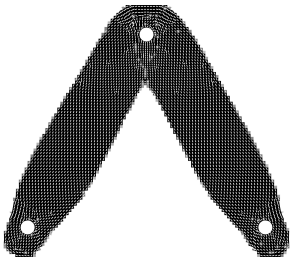

(a) Final results for 40% mass constraint

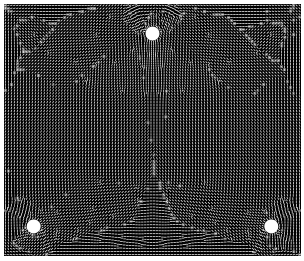

(b) Final results for 100% mass constraint

Figure 6: Final optimal material distribution and orientation results for the 3PT optimization using 40% and 100% mass constraint

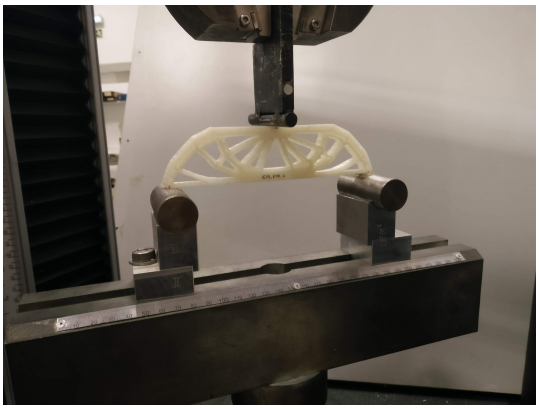

Figure 7: Experimental setup for testing of the printed MBB beam structures

Since using the *Concentric* fiber fill in the structure in Fig. 6(b) results in an undesired fiber layout, a series of 0,1 mm cuts were inserted in the fiber layers, in order to force the slicing program to orient the fibers according to the optimization results, as can be seen in Fig. 9. To minimize the effect of hole deformation during testing, the holes were reinforced in all the core layers with a maximum of five concentric fiber rings. In order to test the printed specimens in a tensile test, special fixtures were machined in order to satisfy the boundary conditions of the optimization problem. The experimental setup is shown in Fig. 10. The results

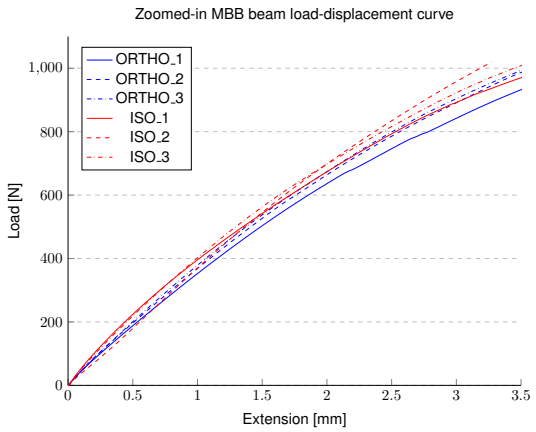

Figure 8: Zoomed-in load-displacement curves for the 3 point bending test of optimized MBB structures

Table 4: Experimental and theoretical stiffness results for the 3 point bending test of optimized MBB structures printed using CFF

MBB Sample	Stiffness $[N/m]\times10^3$	Normalized Stiffness $[N/m]\times10^3$
ORTHO_1	284.06	284.06
ORTHO_2	295.47	295.68
ORTHO_3	293.75	293.96
ISO_1	276.34	286.92
ISO_2	328.33	342.42
ISO_3	294.74	306.14
ORTHO_THEO	940.96	
ISO_THEO	913.04	

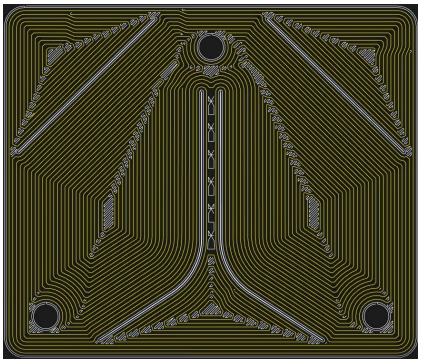

Figure 9: Printing pattern of the 3PT 1,0_Concentric structure

of the experiment can be seen in Fig. 11 and Table 5. By analyzing the load-displacement curves in Fig. 11, several conclusions can be drawn. Since the

Figure 10: Experimental setup for the testing of the 3PT structures

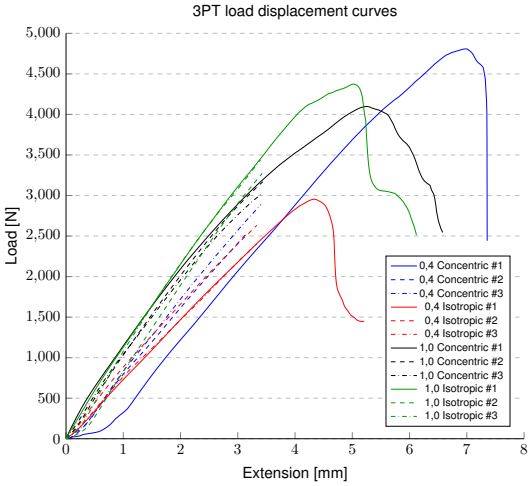

Figure 11: Load-displacement results for the final testing samples of 3PT

ultimate-stress for the 0,4 Concentric structure is greater than the one obtained for the 1,0 Concentric structure, the technique for orienting the fiber with the use of small cut features was not very successful for this problem. The similar ultimate-stress results obtained for the 1,0 structures, which contrast greatly with the results obtained for the 0,4 structures, support this theory, since structures printed with the fiber oriented in the principal stress direction should have an increased ultimate-stress value when compared to structures printed with a quasi-isotropic laminate and using the same amount of fiber. The effect of hole deformation is also possible, revealing that this problem is not the most well

Table 5: Experimental and theoretical stiffness results for the tensile test of optimized 3PT structures printed using CFF

Mass %	Sample	Stiffness [N/m]×10^3	Normalized Stiffness [N/m]×10^3
40	Concentric		
	#1	923.18	2233.20
	#2	815.61	2002.86
	#3	886.58	2170.88
	Theoretical	3780.71	
	Isotropic		
	#1	741.84	1830.95
	#2	774.23	1897.14
	#3	694.64	1715.70
	Theoretical	1895.73	
100	Concentric		
	#1	949.31	949.31
	#2	981.24	992.90
	#3	922.40	934.19
	Theoretical	4653.87	
	Isotropic		
	#1	1023.88	1052.94
	#2	1062.89	1093.39
	#3	1081.17	1108.51
	Theoretical	2443.49	

suited to be tested.

By analyzing the stiffness results in Table 5, several conclusions can be drawn. The experimental results agree with the computational results in that the structures with a higher volume fraction have greater stiffness. Using 40% mass, the Concentric structures are stiffer than the Isotropic structures, as is expected. However, the computational results indicate that the stiffness difference should be twice as much, which is not the case. Using 100% mass, the opposite occurs, with Isotropic structures being stiffer than the Concentric structures, which is not expected. This result could indicate that the employed technique is not useful in this case. When observing the normalized stiffness results, the value of the 40% structures are greater than the 100% structures, almost by a factor of two, since the stiffness results don't increase as much as the weight. This justifies using the 40% mass structures since their stiffness/weight ratio is greater. The results from the experimental tests differ greatly in terms of numerical value from the computational results, which could be explained by the difficulty in simulating the behavior of the sandwich panel, due to the printing process, as the fiber can't be printed in the same disposition as in the optimization results and also because the local hole deformation may not be accounted for in the simulations.

5. Conclusions

The goal of this work was to develop a structural optimization program capable of determining optimal material distribution and orientation for structures created by FFF processes implementing continuous fiber filament. To this end, a Matlab program was developed based on the DMO method, using the MMA optimizer to minimize the compliance of the structure. To allow the study of complex bidimensional structures, the finite mesh generation is performed by the finite element program Siemens Nx, using triangular and quadrilateral finite elements.

To test the developed program, the MBB beam and a three-point tensile problem were optimized in respect to the material distribution and orientation. The studies showed that changing the ratio of Young's modulus has no significant effect on the final structure and material orientation, while changing the shear stiffness can have a significant impact in the material distribution and orientation of the final structures. In order to complement the computational results, experimental testing and characterization of the composite layup was performed and samples of the MBB beam and 3PT structures were printed and tested with fiberglass continuous fiber reinforcement using the Markforged Mark Two 3D printer, to determine their stiffness.

The major findings obtained by the experimental tests can be summarized as:

- Topology optimized structures and material distribution and orientation optimized structures have similar stiffness when printed with fiber oriented along the principal stress directions if the composite material has a shear stiffness similar to an isotropic material ($\beta = 0$).
- Lighter, functional structures have higher stiffness/weight ratio than heavier structures, but lower stiffness overall.
- Structures printed with optimal fiber orientation have better performance than structures printed with generic quasi-isotropic layups for the same fiber volume.
- Conclusions about the proposed fiber orientation technique can't be performed due to improper experimental testing, requiring further examination.
- The experimental results confirm the general findings obtained by the computational results for the MBB beam and 3PT structure, although with lower stiffness results due to the

CFF process limitations and local stress concentration.

5.1. Future Work

Several improvements to the presented work could still be implemented and will be presented here as future work ideas as follows:

- Instead of using the presented parameterization methods, other methods could be used to increase the number of possible orientations without increasing the computation time.
- Use of a discrete "weak" material lead to convergence difficulty. Use of a SIMP like method of using a pseudo-density could prove more useful.
- An Equivalent Single Layer Model (ESLM) was used to simulate the structures. Use of a layer-wise model would be interesting to implement in order to simulate the layer-by-layer behavior of the FFF process and determine which layers should have fiber and its orientation.
- Further experimental studies of the material orientation technique should be implemented using better case studies to assess the practicality of the method.

References

[1] ASTM D 3039/D 3039M – 00, Standard Test Method for Tensile Properties of Polymer Matrix Composite Materials. ASTM International. West Conshohocken, PA, 2002.

[2] M. P. Bendsøe and O. Sigmund. *Topology Optimization: theory, methods and applications*, volume 95. Springer Berlin Heidelberg, Berlin, Heidelberg, 2004.

[3] M. Caminero, J. Chacón, I. García-Moreno, and J. Reverte. Interlaminar bonding performance of 3d printed continuous fibre reinforced thermoplastic composites using fused deposition modelling. *Polymer Testing*, 68:415 – 423, 2018.

[4] M. Caminero, J. Chacón, I. García-Moreno, and G. Rodríguez. Impact damage resistance of 3D printed continuous fibre reinforced thermoplastic composites using fused deposition modelling. *Composites Part B: Engineering*, 148:93–103, 2018.

[5] A. N. Dickson, J. N. Barry, K. A. McDonnell, and D. P. Dowling. Fabrication of continuous carbon, glass and Kevlar fibre reinforced polymer composites using additive manufacturing. *Additive Manufacturing*, 16:146–152, 2017.

[6] R. T. L. Ferreira, I. C. Amatte, T. A. Dutra, and D. Bürger. Experimental characterization and micrography of 3D printed PLA and PLA reinforced with short carbon fibers. *Composites Part B: Engineering*, 124:88–100, 2017.

[7] R. M. Hoglund. An Anisotropic Topology Optimization Method For Carbon Fiber-Reinforced Fused Filament Fabrication. Master's thesis, Baylor University, 2016.

[8] H. P. Jia, C. D. Jiang, G. P. Li, R. Q. Mu, B. Liu, and C. B. Jiang. Topology Optimization of Orthotropic Material Structure. *Materials Science Forum*, 575-578:978–989, 2008.

[9] D. Jiang. Three dimensional topology optimization with orthotropic material orientation design for additive manufacturing structures. Master's thesis, Baylor University, 2017.

[10] T. Nomura, E. M. Dede, J. Lee, S. Yamasaki, T. Matsumori, A. Kawamoto, and N. Kikuchi. General topology optimization method with continuous and discrete orientation design using isoparametric projection. *International Journal for Numerical Methods in Engineering*, 101(8):571–605, 2015.

[11] T. Nomura, E. M. Dede, T. Matsumori, and A. Kawamoto. Simultaneous Optimization of Topology and Orientation of Anisotropic Material using Isoparametric Projection Method. *11th World Congress on Structural and Multidisciplinary Optimization*, 2015.

[12] N. Olhoff, M. P. Bendsøe, and J. Rasmussen. On CAD-integrated structural topology and design optimization. *Computer Methods in Applied Mechanics and Engineering*, 89(1-3):259–279, 1991.

[13] P. Pedersen. Optimal Orientation of Anisotropic Materials Optimal Distribution of Anisotropic Materials Optimal Shape Design with Anisotropic Materials Optimal Design for a Class of Non-Linear Elasticity. In *Optimization of Large Structural Systems*, volume II, pages 649–681. Springer Netherlands, Dordrecht, 1993.

[14] R. Sørensen and E. Lund. In-plane material filters for the discrete material optimization method. *Structural and Multidisciplinary Optimization*, 52(4):645–661, 2015.

[15] J. Stegmann. *Analysis and optimization of laminated composite shell structures*. PhD thesis, Aalborg University, 2004.

[16] K. Svanberg. The method of moving asymptotes—a new method for structural optimization. *International Journal for Numerical Methods in Engineering*, 24(2):359–373, 1987.